





## RESEARCH ARTICLE

## One-Pot Synthesis of Antibacterial and Antioxidant Self-Healing Bioadhesives Using Ugi Four-Component Reactions

Ronak Afshari¹ 📵 | Arpita Roy¹ | Saumya Jain¹ | Kaimana Lum¹ | Joyce Huang¹,² | Sam Denton² | Nasim Annabi¹,² 📵

<sup>1</sup>Department of Chemical and Biomolecular Engineering, University of California, Los Angeles, Los Angeles, California, USA | <sup>2</sup>Department of Bioengineering, University of California, Los Angeles, Los Angeles, California, USA

Correspondence: Nasim Annabi (nannabi@ucla.edu)

Received: 24 September 2024 | Revised: 14 March 2025 | Accepted: 5 April 2025

Funding: This work was supported by National Institutes of Health (Grant Nos. R01-EB023052 and R01-HL140618).

Keywords: adhesive hydrogel | antibacterial property | antioxidant property | self-healing | Ugi four-component reaction | viscoelasticity | wound repair

#### **ABSTRACT**

Bioadhesive materials are extensively utilized as alternatives to surgical sutures and wound dressings. Despite significant advancements in their synthesis, current bioadhesives suffer from inadequate mechanical stability, suboptimal wet tissue adhesion, and a lack of inherent antibacterial and antioxidant properties, while requiring multistep synthesis processes, complicating their production for biomedical applications. To address these limitations, we developed a new bioadhesive, named UgiGel, synthesized through a one-pot Ugi four-component reaction (Ugi-4CR). Our strategy utilized gelatin as the backbone, 4-formylphenylboronic acid (4-FPBA) as an aldehyde source for improved adhesion and antibacterial activity, gallic acid (GA) as a carboxylic acid source for improved antioxidant activity and wound healing, and cyclohexyl isocyanide (CyIso) to induce pseudopeptide structures. The internal crosslinking between GA and 4-FPBA via dynamic boronate ester bond formation, triggered by slight pH changes (7.4–7.8) and temperature elevation (25°C-40°C), resulted in the formation of viscoelastic and self-healing hydrogels with water as the only byproduct without the need for initiator/light activation. UgiGel showed higher adhesion to porcine skin tissue (139.8 ± 8.7 kPa) as compared to commercially available bioadhesives, Evicel (26.3 ± 2.6 kPa) and Coseal (19.3 ± 9.9 kPa). It also demonstrated effective antibacterial properties against both Gram-negative and Gram-positive bacteria, as well as antioxidant activity. Additionally, the in vitro studies using NIH-3T3 cells confirmed the biocompatibility of the UgiGel over 7 days of culture. Moreover, in vivo biocompatibility and biodegradation of UgiGel were confirmed via subcutaneous implantation in rats for up to 28 days. Our results demonstrated that UgiGel outperformed commercially available bioadhesives in terms of adhesion, self-healing, and antibacterial activity, without compromising biocompatibility or physical properties, representing a promising multifunctional bioadhesive for wound sealing and repair.

### 1 | Introduction

The increasing demand for rapid and effective wound sealing and repair has driven the development of multifunctional bioadhesives with strong wet tissue adhesion, antibacterial, and antioxidant properties, designed for on-demand treatment [1].

However, despite significant advancements and the steady flow of innovative research in this field, creating bioadhesives that combine all the necessary properties for wound management, such as mechanical integrity, high adhesive strength, elasticity, antibacterial properties, and biocompatibility within a single structure, remains a major challenge [2, 3]. For

© 2025 Wiley Periodicals LLC.

instance, despite the high biocompatibility and degradability of fibrin-based glues (e.g., Evicel, Tisseel), they have demonstrated poor adhesion under wet conditions in the body and an increased chance of virus transmission [4]. Strong adhesives such as cyanoacrylates have high adhesive strength but are much stiffer than the native tissues and contain toxic agents or release toxic byproducts upon degradation [5]. On the other hand, bioadhesives that possess all the desired properties typically involve multiple polymeric components and laborious fabrication steps, limiting their practical application [6, 7]. For example, biomimetic hydrogel-based adhesives exhibit adequate adhesion strength and can maintain a moist environment while aiding in the removal of necrotic tissue [8]. However, they often require dual polymeric networks or the incorporation of nanoparticles (NPs) to achieve sufficient mechanical strength [9-11]. In addition, most of the bioadhesives require complex multistep synthesis routes [12] and/or the use of external stimuli for crosslinking, including lights and chemical crosslinkers [13, 14]. Therefore, there is an unmet need for a multifunctional bioadhesive that concurrently provides wet tissue adhesion and antimicrobial efficacy at the wound site and can be synthesized through a one-step reaction without the need for sequential purification and/or the use of light/catalyst/crosslinker.

To address this limitation, multicomponent reactions (MCRs) [15, 16] can be used as a cutting-edge approach to create complex multifunctional architectures with minimal synthetic steps [17]. These reactions combine three or more starting materials in a single vessel to produce a product through a cascade or domino process, without the need for isolation or purification of any intermediates, resulting in lowered cost and waste [18]. Among MCRs, the Ugi four-component reaction (Ugi-4CR) is particularly notable for its versatility and efficiency [19], due to the ability to form pseudopeptide products with amide bonds that can mimic peptides and proteins found in biological systems, with water as the only byproduct [20]. Ugi-4CR combines a carboxylic acid, an amine, a carbonyl compound, and an isocyanide, yielding α-acetamido carboxamide derivatives under mild reaction conditions such as room temperature and non-inert atmosphere (Figure 1A) [21].

The Ugi-4CR approach has been employed to functionalize carbonaceous materials both noncovalently [22] and covalently for applications in drug [23] and gene delivery [24]. Afshari et al. reported the functionalization of phthalocyanines via Ugi-4CR, demonstrating their potential as potent photosensitizers in cancer therapy [25]. Additionally, natural polymers such as cellulose and chitosan (CS) have been modified using Ugi-4CR with various proteins for vaccine development [26] and enzyme immobilization [27]. The Ugi-4CR approach has also been utilized for the synthesis of gelators with phenylboronic acid (PBA) motifs, which can react with diol-containing polymers like polyvinyl alcohol (PVA) to form antibacterial and self-healing hydrogels [28, 29]. Moreover, the applicability of the Ugi-4CR for the total synthesis of natural products and their analogs was investigated in detail [30]. These findings highlight the considerable potential of Ugi-4CR to enhance material properties for various biomedical applications.

In this study, for the first time, we used Ugi-4CR to engineer a multifunctional bioadhesive by integrating various small and large molecules with different properties in a one-pot synthesis. The engineered gelatin-based self-healing, antibacterial, and antioxidant bioadhesive, named UgiGel, was formed without the need for complex synthesis, light activation, catalysts, or post-purification steps. UgiGel was formed utilizing gelatin as the amine source, 4-formylphenylboronic acid (4-FPBA) as the aldehyde source, gallic acid (GA) as the carboxylic acid source, and cyclohexyl isocyanide (CyIso) as the isocyanide component (Figure 1B). A key feature of the design is the dynamic chemistry between the phenolic groups of GA and the boronic motifs of 4-FPBA, which act as an internal crosslinking tool. The ability of these linkages to break and reform under specific conditions imparts UgiGel with smart self-healing properties. The designed Ugi-4CR can produce a highly viscoelastic and adhesive hydrogel, where the hydroxyl groups of GA and PBA can enhance adhesion to tissue. Also, the polyphenolic groups of 4-FPBA and GA contribute to the antibacterial properties and antioxidant activity to control wound inflammation. To demonstrate the clinical applicability of UgiGel, we evaluated the in vitro cytotoxicity and in vivo biocompatibility and biodegradability using NIH 3T3 cells and subcutaneous implantation into the dorsal skin of rats, respectively.

### 2 | Materials and Methods

#### 2.1 | Materials

Gelatin from porcine skin was purchased from Sigma-Aldrich (Bloom 300, type A, Sigma). 4-FPBA was obtained from Merck. GA, CyIso, methacrylic anhydride, triethanolamine (TEA), N-vinyl caprolactam (VC), Eosin Y disodium, paraformaldehyde, Triton X-100, 2,2-diphenyl-1-picrylhydrazyl (DPPH), and polydimethylsiloxane (PDMS) were sourced from Sigma-Aldrich. Dulbecco's phosphate-buffered saline (DPBS) was acquired from Fisher Scientific (USA). Dulbecco's Modified Eagle Medium (DMEM) was purchased from Cellgro (Manassas, VA), and fetal bovine serum (FBS) was obtained from HyClone (Logan, UT). DMSO-d6 was purchased from Cambridge Isotope Laboratories Inc. All reagents were used as received without further purification. Commercial live/dead kits, AlexaFluor 488 (phalloidin), and 4',6-diamidino-2-phenylindole dihydrochloride (DAPI) were purchased from Invitrogen. Mayer's hematoxylin was purchased from Electron Microscopy Sciences.

### 2.2 | Synthesis of UgiGel

In a typical procedure, gelatin (0.51 g, 5.00 mmol) was mixed with 20 mL water and heated at 50°C to be dissolved. Then, aldehyde (4-FPBA: 0.74 g, 5.00 mmol; 3,4-dihydroxybenzaldehyde: 0.69 g, 5.00 mmol) was added to the solution, followed by the addition of 25 mL ethanol (EtOH). The solution was stirred at room temperature for 1 h. Then, CyIso (0.54 g, 5.00 mmol) and GA (0.85 g, 5.00 mmol) were added, and the resulting mixture was stirred at room temperature for 24 h in a closed vial [31]. Finally, the reaction temperature was increased to 40°C for

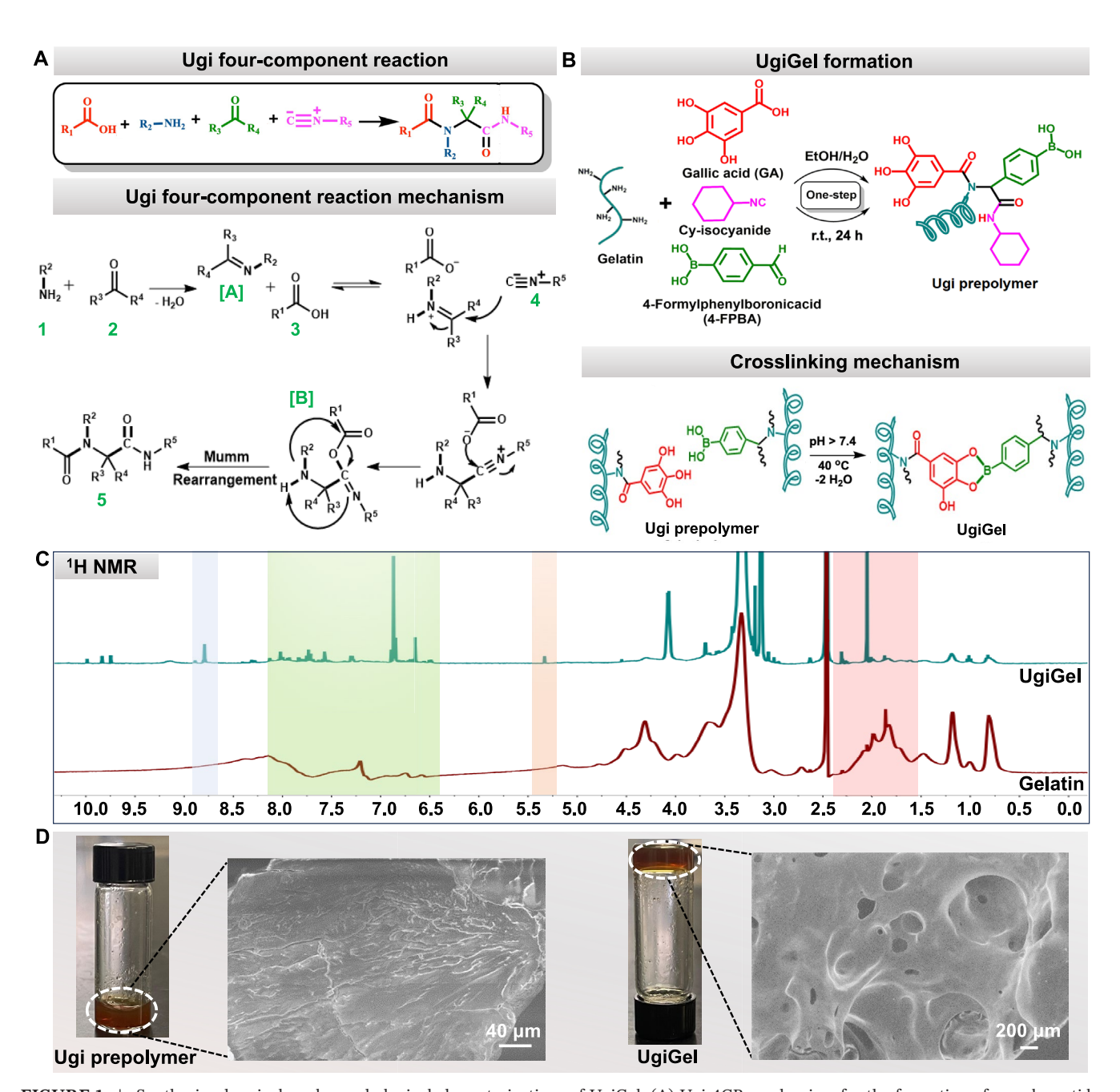


**FIGURE 1** | Synthesis, chemical, and morphological characterizations of UgiGel. (A) Ugi-4CR mechanism for the formation of pseudopeptide structures through the reaction of amine, carboxylic acid, aldehyde, and isocyanide components. (B) Schematic illustration of UgiGel formation through the functionalization of gelatin via Ugi-4CR and subsequent crosslinking. (C)  $^{1}$ H NMR spectrum comparison of UgiGel and gelatin. (D) Representative SEM images of Ugi prepolymer and crosslinked UgiGel (scale bar: 40 and 200  $\mu$ m).

1 min, and the pH was fixed to 7.4–7.8 to form a crosslinked UgiGel by forming dynamic boronate ester bonds in the hydrogel network. On completion, the reaction mixture cooled to room temperature, and UgiGel was purified by washing with EtOH/acetone and isolated by centrifugation (20,000 rpm, 10 min, five times).

## 2.3 | Synthesis of Gelatin Methacryloyl (GelMA) Hydrogel

GelMA, as a control, was synthesized as described previously [32]. In brief, 15.00g of porcine skin gelatin was dissolved in

150 mL DPBS under vigorous stirring at 55°C for 1 h. Then, 8 mL of methacrylic anhydride was added dropwise to the gelatin solution under continuous stirring at 50°C for 3.5 h. The solution was then diluted with DPBS and dialyzed against deionized water at 50°C for 5 days. The resulting solution was then filtered and lyophilized for 3 days. The photoinitiator solution was prepared by dissolving TEA [1.875% (w/v)], 1.25% (w/v) VC, and Eosin Y disodium salt (0.50 mM) in distilled water at 37°C. GelMA precursor solutions were prepared by dissolving varying concentrations of GelMA [10% and 20% (w/v)] in the photoinitiator solution. Then, the solution was photocrosslinked for 4 min with visible light (450–550 nm) by using an LS1000 Focal Seal Xenon Light Source (100 mW/cm², Genzyme).

# 2.4 | Chemical and Morphological Characterization of UgiGel

The chemical structure of UgiGel was confirmed by proton nuclear magnetic resonance (¹H NMR) spectroscopic analysis using a 400MHz Bruker AV400 spectrometer. For ¹1H NMR analysis, UgiGel and gelatin samples were prepared by dissolving 10 mg of each one in 1 mL of DMSO solvent. Scanning electron microscopy (SEM) observations were carried out using a scanning electron microscope (ZEISS Supra 40VP SEM) to gain insight into the structure and morphology of UgiGel. The Ugi prepolymer and UgiGel samples were lyophilized for 48 h and mounted onto SEM stubs, coated with a 60-s application of gold via sputtering, and then visualized.

# 2.5 | Rheological and Mechanical Characterization of UgiGel

The gel properties (viscosity, shear-thinning, and self-healing) of the newly designed UgiGel were characterized using an Anton-Paar 302 Rheometer [33, 34]. The crosslinked UgiGel samples were analyzed using an 8 mm parallel plate geometry with a 0.1 mm gap at 37°C  $\pm$  2°C. Storage (G') and loss (G'') moduli were measured through amplitude sweeps over a strain range of 0.05%–140% and frequency sweeps ranging from 5 to 40 Hz. The viscosity of UgiGel was measured with an increase in shear rate ranging from 0.1 to  $1000\,\mathrm{s^{-1}}$ . Additionally, a cyclic strain sweep test was conducted, alternating between % and 100% strain over time, to explore the self-healing capability of UgiGel.

### 2.6 | In Vitro Degradation Studies

In vitro degradation studies were conducted over 42 days in DPBS using UgiGel hydrogels, which were fabricated by casting the Ugi prepolymer into 8 mm circular PDMS molds, followed by placing the mold in a temperature-controlled oven at 40°C for 1 min with adjusted pH. The hydrolytic degradation profiles were evaluated in the physiological condition (37°C and pH: 7.4). Each sample was weighed ( $W_0$ ) and immersed in DPBS. After a predetermined time interval (up to 42 days), the sample was rinsed in MilliQ water three times and weighed ( $W_t$ ) after freeze-drying. The degradation rate was then calculated using Equation (1):

Degradation rate (%) = 
$$\frac{W_0 - W_t}{W_0} \times 100$$
 (1)

#### 2.7 | Swelling Ratio Determination

The swelling behavior of the UgiGel was evaluated by weighing the gels before and after immersion in DPBS. Ugi prepolymer was cast into 8 mm PDMS molds, followed by thermal gelation in the oven at 40°C for 1 min with adjusted pH, after which their initial weights were recorded. They were then submerged in DPBS at 37°C, with their weights monitored over time. The swelling ratio was calculated using Equation (2), where  $W_0$  represents the initial mass and  $W_i$  represents the mass of the hydrogel at various time points.

Swelling ratio (%) = 
$$\frac{W_i - W_0}{W_0} \times 100$$
 (2)

#### 2.8 | In Vitro Adhesive Properties of UgiGel

The in vitro adhesive properties of the UgiGel were investigated based on standard wound closure (ASTM-F2458-05) and burst pressure (ASTM-F2392-04) tests and compared to commercially available sealants, including a fibrin-based sealant (Evicel) and a poly(ethylene glycol) (PEG)-based sealant (Coseal). A wound closure test was performed to determine the adhesive strength of the UgiGel using porcine skin samples, as explained before [12]. For this purpose, skin samples were carefully cut into 1 cmlength pieces and moisturized with DPBS. Then at their intersection points, Ugi prepolymer was placed and crosslinked using heating at 40°C for 1 min and adjusting the pH. Two free ends of the tissue were then attached to glass slides using superglue with a 0.50cm overhang. The glass slides were then mounted on the Instron 5943 mechanical tester, and tensile loading was conducted at a strain rate of 1 mm/min until failure. The adhesive strength was determined by recording the maximum stress at the point of tissue detachment, as indicated on the stressstrain curve.

For the in vitro burst pressure test, first, collagen sheets were submerged in water to simulate skin tissue and loaded into airtight stainless-steel plates where the upper plate had a 10 mm diameter opening [35]. An 18G needle was used to prepare a puncture in the collagen sheet before the Ugi prepolymers were applied and heated up to 40°C for 1 min with adjusted pH over the defect. Next, air was continuously pumped into the system at a rate of 10 mL/min using a syringe pump (Syringe Pump NE-1000). Pressure data were recorded using a PASCO wireless pressure sensor and Capstone software. The system was pressured until the UgiGel burst was observed as the escape of bubbles from the defect site.

#### 2.9 | In Vitro Antibacterial Activity of UgiGel

The bacterial test was performed using two bacterial strains: Pseudomonas aeruginosa (Gram-negative) and methicillinresistant Staphylococcus aureus (MRSA) (Gram-positive) [36]. P. aeruginosa was cultured by inoculating a streak plate with the nonoverlapping zigzag method on Luria-Bertani (LB) agar plates, followed by incubation at 37°C overnight. S. aureus was cultured similarly, using Tryptic Soy Agar (TSA) plates. After overnight incubation at 37°C, a single colony from each bacterial strain was suspended in its respective growth broth and incubated at 37°C overnight. The following day, the optical density (OD) of each bacterial suspension was adjusted to 0.06-0.08 at 625 nm. UgiGel and gelatin samples were introduced into the bacterial suspensions and incubated at 37°C, with a control group containing only bacteria without hydrogel. Bacterial density and viability were monitored by measuring OD at 625 nm using a Biotek Eon Microplate Spectrophotometer. The antibacterial activity was assessed on days 2 and 7 using colony-forming unit (CFU) assays to determine bacterial viability.

#### 2.10 | In Vitro Antioxidant Efficacy of UgiGel

The free radical scavenging activity of UgiGel was assessed using the DPPH assay [37, 38]. UgiGel samples (500.00 mg) were dispersed in 5 mL of water, then 0.20 mL of a 1.75 mM DPPH solution in ethanol was added and mixed. The mixture was then incubated in the dark for 30 min. The DPPH scavenging efficiency of UgiGel was determined by measuring the absorbance at 535 nm using a TECAN M200 Pro plate reader. The percentage of DPPH scavenging was calculated using Equation (3):

DPPH scavenging (%) = 
$$\frac{Abs_c - Abs_s}{Abs_c} \times 100$$
 (3)

where  ${\rm Abs}_{\rm c}$  represents the absorption of control (DPPH in ethanol/water), and  ${\rm Abs}_{\rm s}$  represents the absorption of the UgiGel-DPPH in ethanol/water.

### 2.11 | In Vitro Cytocompatibility of UgiGel

The cytocompatibilities of the UgiGel and GelMA (10%, w/v) bioadhesive as a control were evaluated using NIH 3T3 fibroblast cells (CRL-1658, ATCC) [39]. The cells (cell density: 2700 cells/ cm2) were 2D seeded on UgiGel and GelMA and cultured at 37°C in 5% CO<sub>2</sub> in DMEM media supplemented with 10% FBS and 1% antibiotics, where media was refreshed every 2 days. On days 1, 3, and 7 of the culture, live/dead staining using commercial live/ dead kits (calcein AM and ethidium homodimer-1) as well as Factin/DAPI staining using Alexa Fluor 488 Phalloidin and DAPI (Invitrogen, San Diego, CA) were conducted to monitor cell viability, morphology, and density. Cell viability was quantified after live (cells stained green) and dead (cells stained red) staining by determining the percent of live cells over total cells. The morphology of the 2D seeded cells on UgiGel was analyzed, and cell number was quantified after F-actin (cytoskeleton stained green) and DAPI (nuclei stained blue) staining by determining the amount of positively stained nuclei per unit area [40]. Briefly, F-actin/DAPI staining was conducted by fixing the cells in 4% (v/v) paraformaldehyde, permeabilizing in 0.10% (w/v) Triton X-100, blocking in 5% donkey serum, and incubating with Alexa Fluor 488 Phalloidin and DAPI in donkey serum. Both staining results were imaged using an inverted fluorescence microscope (Zeiss Axio Observer Z7) and processed using ImageJ software.

## 2.12 | In Vivo Biocompatibility and Biodegradation Studies

The animal studies were approved by the IACUC (protocol ARC-2021-113) at UCLA. Subcutaneous implantation and subsequent immunohistochemical analysis were performed according to our previously published methods [41]. Male Wistar rats (250–300g) were purchased from Charles River Laboratories (Boston, MA) and anesthetized by inhalation of isoflurane (~2%), which was maintained throughout the procedure. After anesthesia, eight 1 cm incisions were made on the dorsal skin of the rats, and small subcutaneous pockets were prepared using blunt scissors. Lyophilized UgiGel and GelMA (20%, w/v) samples were implanted into the pockets, and the incisions were

closed with 4-0 polypropylene sutures (Ad Surgical) (n=4). At days 7 and 28 post-operation, the rats were euthanized, and the implanted hydrogels were harvested with the surrounding tissue. Histological analysis was performed to evaluate the inflammatory response in subcutaneous tissue caused by the implanted hydrogels. After retrieving the hydrogels with surrounding tissue, the samples were fixed in 4% paraformaldehyde for 4h and incubated at 4°C in 15% and 30% (w/v) sucrose solution, respectively. The samples were then embedded in an optimal cutting temperature (OCT) compound, frozen in liquid nitrogen, and sectioned using a Leica CM1950 cryostat machine. The 10 µm sections were then mounted on positively charged slides and processed for hematoxylin and eosin (H&E) (Electron Microscopy Sciences) staining and immunostaining for macrophages (CD68) and nuclei (DAPI), which were done according to manufacturer instructions. Anti-CD68 (ab125212) (Abcam) was utilized as a primary antibody, while Goat anti-Rabbit IgG (H+L) antibody conjugated to Alexa Fluor 488 (Invitrogen) was used as a detection reagent and secondary antibody. All the antibodies were validated on respective hosts by the manufacturer and used in this study without further purification.

Cell infiltration was quantified based on H&E images of UgiGel and GelMA hydrogels 7- and 28-days post-implantation into rat dorsal tissue. The area of the hydrogel was measured, and the number of hematoxylin-stained cell nuclei (blue/purple in color) present within the hydrogel matrix was counted using ImageJ software. These data were used to calculate cell infiltration per area of hydrogel (cells/cm²) (n=3). Macrophage infiltration was quantified from immunostaining images of CD68 and DAPI-stained hydrogel-tissue intersections following subcutaneous implantation. The tissue area and the number of CD68-stained cells (red in color) were analyzed using ImageJ software. Then, the macrophage infiltration into the tissue was calculated as a measure of cells/cm² (n=3) [42, 43].

#### 2.13 | Statistical Analysis

Statistical analysis of all numerical data was carried out using an ANOVA test with GraphPad Prism software. For each experiment, at least three samples were tested, and data were presented as means  $\pm$  standard error of the mean (SEM) (\*p<0.05, \*\*p<0.01, \*\*\*p<0.001, and \*\*\*\*p<0.0001).

#### 3 | Results

#### 3.1 | Design and Synthesis of UgiGel

UgiGel bioadhesive was synthesized through a Ugi-4CR, employing gelatin (as the amine source), 4-FPBA (as the aldehyde source), GA (as the carboxylic acid source), and CyIso in a fixed 1:1:1:1 M ratio. According to the commonly accepted Ugi reaction mechanism described in Figure 1A, amine source 1 (gelatin), aldehyde source (4-FPBA) 2, and carboxylic acid 3 (GA) 3 were in equilibrium with imine [A] in the reaction medium. The addition of CyIso 4 onto the iminium group, followed by the addition of the carboxylate ion onto the C atom of the nitrilium ion, led to the formation of the adduct [B], which underwent an

intramolecular acylation known as the Mumm rearrangement to give the stable Ugi prepolymer 5. The Ugi prepolymer exhibited viscoelastic and gel-like characteristics due to the extensive network of hydroxyl groups of GA and 4-FPBA, present on the amine backbone of gelatin. These hydroxyl groups facilitated strong intermolecular hydrogen bonding, contributing to the formation of a highly interconnected polymer network and imparting viscoelastic properties to the Ugi prepolymer. Then, the UgiGel prepolymer was crosslinked by increasing the temperature from 25°C to 40°C for 1 min and adjusting the pH to above the pKa of 4-FPBA (pH: 7.4), leading to the formation of an elastic UgiGel hydrogel in the reaction medium (Figure 1B).

The successful formation of the UgiGel was verified via  $^1H$  NMR analysis, confirming the presence of the characteristic peak for UgiGel compared to pure gelatin (Figure 1C). The indication of a singlet for the methine proton of the  $\alpha$ -acetamido carboxamide derivatives ( $\delta$ =5.3 ppm, highlighted in orange) and multiplets in the aromatic region ( $\delta$ =6.4–8.1 ppm, highlighted in green) corresponded to the aromatic protons from the aryl group of GA and 4-FPBA, respectively. Additionally, sharp signals around 8.6–8.8 ppm (highlighted in blue), originating from the amide moieties, were observed, along with methylene and methine peaks between 1.5 and 2.4 ppm (highlighted in red), which were attributed to the aliphatic CyIso components and gelatin backbone.

To further investigate the specific role of boronic groups in the internal crosslinking process, we conducted an additional reaction in which 4-FPBA was replaced with 3,4-dihydroxybenzaldehyde (same aldehyde without boronic groups). The resulting gel exhibited a distinct appearance compared to UgiGel prepared with 4-FPBA. Notably, the gel was white rather than yellowish, and despite heating at 40°C for over 10 min and increasing the pH from 7.4 to 9 (above pKa of 3,4-dihydroxybenzaldehyde), it remained agglomerated instead of forming a stable gel (Figure S1). A vial inversion test was used to assess the stability of both gels, revealing that the gel formed with 3,4-dihydroxybenzaldehyde was weak and presented as an aggregated precipitate, while UgiGel prepared with 4-FPBA was robust after 1 h (Figure S1A,B). Even after adjusting pH to 9, no significant crosslinking occurred in the gel prepared with 3,4-dihydroxybenzaldehyde (Figure S1C) confirming that boronate ester formation was essential for creating a stable gel.

Moreover, SEM analysis was performed to gain insight into the structure and morphology of the Ugi prepolymer and UgiGel after internal crosslinking (Figure 1D). The representative SEM image of Ugi prepolymer showed a relatively flat surface, caused by the presence of condensed non-covalent hydrogen bonding interactions within the gelatin matrix, due to the high density of hydroxyl and amine groups or partial aggregation of functionalized gelatin components. In contrast, the representative SEM image of UgiGel revealed a uniform, porous structure with welldefined and smooth voids of varying sizes, attributed to the dynamic boronate ester bonds formed between the cis-diol groups of GA and the boronic groups of 4-FPBA. This shift in structure reflects the successful formation of a robust and stable hydrogel network through the Ugi-4CR. The pores in the crosslinked UgiGel structure also provided insight into the self-healing capability of UgiGel, since the porous morphology can support the

ability of UgiGel to withstand deformation and recover after mechanical stress.

### 3.2 | Mechanical Properties and Self-Healing Capability of the UgiGel

The rheological analysis of the synthesized UgiGel demonstrated that at strain  $\leq 10\%$ , the storage modulus (G') was significantly higher than the loss modulus (G''), confirming the formation of a viscoelastic hydrogel (Figure 2A). In the amplitude sweep experiment, initially, G' was higher than G'', which is a characteristic of a gel-like structure. However, at a strain of  $\sim 30\%$ , G' and G'' crossed over, indicating a breakdown of the developed gel network. As the % strain increased, both moduli remained parallel with slight variation until reaching a yield point, where the values dropped abruptly. This transition from a gel to a quasi-liquid state suggests localized viscous behavior, likely due to the breakdown of hydrogen bonding within the hydrogel matrix. In the frequency sweep experiment (Figure 2B), G' remained consistently higher than G'' across the entire frequency range, with both moduli showing minimal dependence on frequency. This stability indicated a strong and stable gel network with no observed elastic-viscous crossover, further demonstrating the presence of an entangled network within UgiGel. This gel behavior resembled chemically crosslinked hydrogels more than physically crosslinked ones, likely due to internal boronate ester linkages contributing to its structural stability. As shown in Figure 2C, the hydrogel exhibited shear-thinning behavior, where viscosity decreased with increasing shear rate, indicating non-Newtonian fluid characteristics.

UgiGel also exhibited remarkable self-healing capabilities, as evidenced by a cut-and-heal test (Figure 2D). Initially, the hydrogel was bisected using scissors (Figure 2D, Cut), and the separated halves were placed in contact along the fracture interface (Figure 2D, Contact). Without the application of external stimuli, the hydrogel exhibited autonomous self-healing at room temperature. The gel showed complete integration (Figure 2D, Self-healing) and maintained stretchability without rupture after 10 min. The restored sample preserved structural integrity and mechanical resilience, as confirmed by its ability to withstand stretching even after 48 h, with no signs of breakage along the contact line (Figure 2D, Stretching). The observed self-healing could be attributed to the dynamic, reversible boronate-ester linkages present within the UgiGel network, facilitating rapid reformation of covalent interactions. To further confirm the self-healing capability of UgiGel, rheological cyclic strain sweep experiments (Figure 2E) were performed, demonstrating its rapid recovery following mechanical deformation. Upon application of high strain (100%), the gel experienced a significant reduction in viscosity, indicating structural disruption. However, upon removal of strain (1%), the viscosity returned to near its initial value, reaffirming its robust self-healing mechanism. Notably, this recovery remained highly consistent across multiple deformation cycles, showcasing its ability to endure repeated mechanical stress without permanent loss of integrity. The rapid and efficient restoration of viscosity, coupled with minimal hysteresis between successive cycles, underscores the dynamic

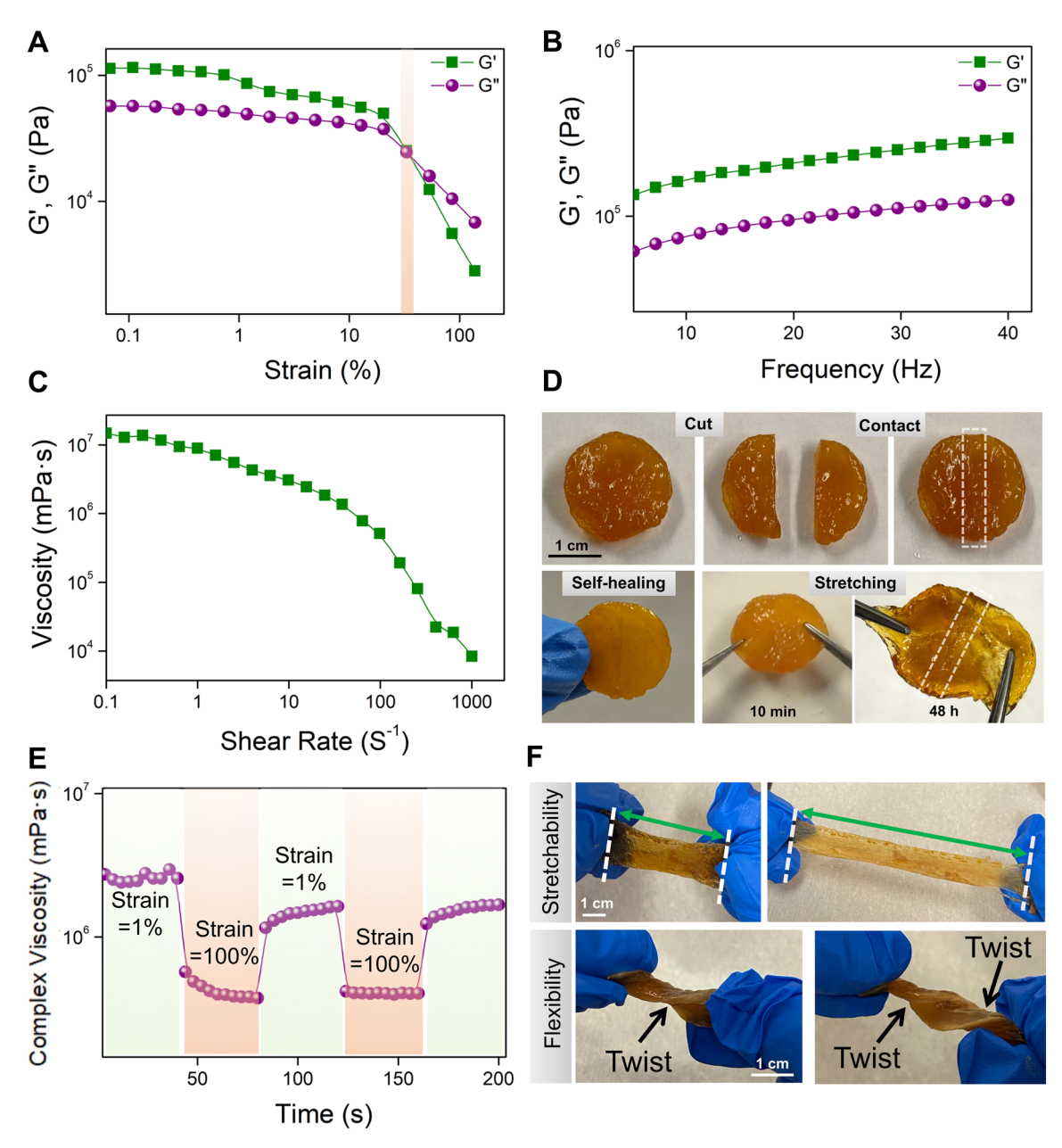


**FIGURE 2** | Rheological and self-healing characteristics of UgiGel. (A) Amplitude sweep experiment. (B) Frequency sweep measurement. (C) Viscosity measurement of UgiGel as a function of shear rate. (D) Visual demonstration of self-healing properties of UgiGel. (E) Cyclic strain sweep experiment confirming the self-healing nature of UgiGel. (F) Mechanical flexibility and stretchability of UgiGel (n = 3, scale bar: 1 cm).

reversibility of the internal network interactions within UgiGel, highlighting its ability to rebuild its structure and consistency after being subjected to external stress. Finally, Figure 2F highlights the stretchability and flexibility of the asprepared UgiGel, as demonstrated by its ability to withstand both stretching and twisting forces without breaking.

# 3.3 | In Vitro Degradation and Swelling Behavior of UgiGel

We evaluated the degradation of UgiGel in DPBS at a physiological pH of 7.4°C and 37°C. As shown in Figure S2A, UgiGel demonstrated a gradual degradation with  $76.6\% \pm 1.2\%$ 

degradation observed at the end of the 42-day timeframe. We next investigated the swelling behavior of UgiGel by weighing the gels before and after immersion in DPBS at pH 7.4. The swelling ratio consistently increased from ~0% to  $45.3\% \pm 2.6\%$  within 10 h and remained stable until  $48 \, \text{h} \, (46.7\% \pm 1.7\%)$  (Figure S2B).

## 3.4 | In Vitro Adhesive Properties of the UgiGel

The adhesion properties of UgiGel were assessed through ASTM (American Society for Testing and Materials) standard tests for in vitro wound closure and ex vivo burst pressure. In vitro wound closure adhesion test was performed to determine the adhesive strength of UgiGel to porcine skin

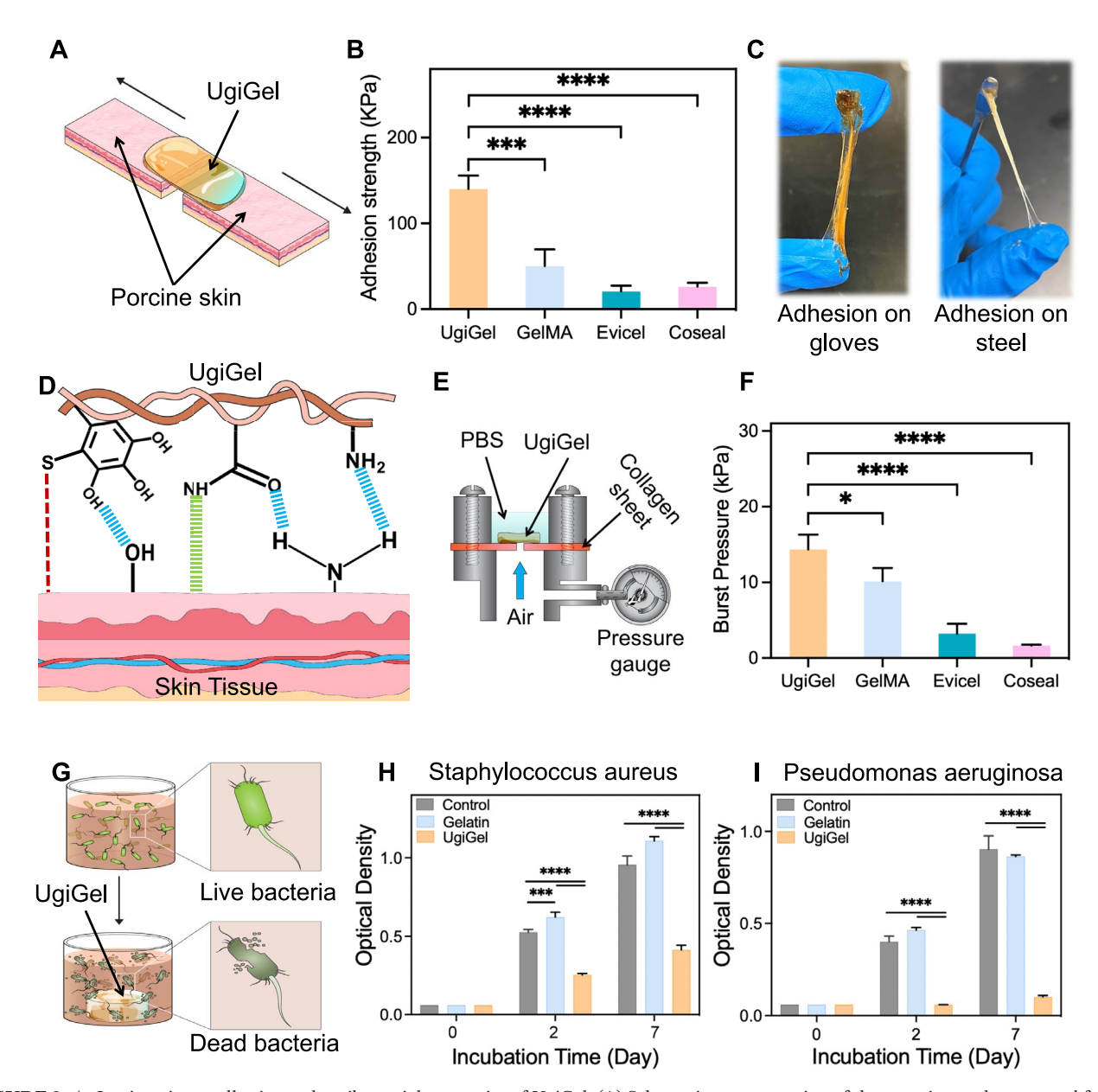


**FIGURE 3** | In vitro tissue adhesive and antibacterial properties of UgiGel. (A) Schematic representation of the experimental setup used for the wound closure test on porcine skin. (B) Quantitative comparison of the adhesion strength of UgiGel to GelMA bioadhesive and other commercial bioadhesives, showing significantly higher adhesive strength for UgiGel (n=3). (C) Digital images illustrating the adhesive properties of UgiGel on different surfaces, including plastic and steel. (D) Proposed adhesion mechanism of UgiGel to wet tissue surfaces. (E) Schematic demonstration of the experimental setup for the burst pressure test using a collagen sheet to mimic tissue conditions. (F) Quantitative comparison of the burst pressure of UgiGel with GelMA bioadhesive and other commercial bioadhesives, demonstrating the superior performance of UgiGel (n=3). (G) Antibacterial activity of the UgiGel against (H) *S. aureus* (Gram-positive) and (I) *P. aeruginosa* (Gram-negative) bacteria (control: bacteria without hydrogel) (n=3) (\*p<0.05, \*\*\*p<0.001, \*\*\*\*p<0.0001).

(Figure 3A) [12]. The results confirmed that the adhesion strength of UgiGel was significantly higher compared to both GelMA bioadhesive (20%, w/v) and commercial sealants Evicel and Coseal, as shown in Figure 3B. UgiGel exhibited an average adhesion strength of  $139.8\pm8.7\,\mathrm{kPa}$ , which was more than double the adhesion strength of GelMA ( $46.9\pm8.5\,\mathrm{kPa}$ ) and more than five times that of Coseal ( $26.3\pm4.7\,\mathrm{kPa}$ ) [41] and Evicel ( $20.8\pm6.7\,\mathrm{kPa}$ ) [41]. Interestingly, as-prepared UgiGel showed strong adhesion to different surfaces like gloves and steel (Figure 3C). The high adhesion strength

could be attributed to the enrichment of UgiGel with a large amount of phenolic, hydroxyl, amine, and amide functional groups that can react with tissue functional groups such as carboxyl, hydroxyl, and amine groups (Figure 3D).

In vitro burst pressure experiments were also conducted to check the sealing ability of UgiGel for the wound under air or liquid pressures, using punctured and pressurized skin-mimicking collagen sheets (Figure 3E). The burst pressure of UgiGel was shown to be  $14.3\pm1.1\,\mathrm{kPa}$ , which was higher than GelMA

bioadhesive  $(10.1\pm1.0\,\text{kPa})$  and commercial sealants including Coseal  $(1.7\pm0.1\,\text{kPa})$  [41] and Evicel  $(3.2\pm1.3\,\text{kPa})$  [41] (Figure 3F).

#### 3.5 | In Vitro Antibacterial Activity of the UgiGel

An in vitro antibacterial assay experiment was performed to assess the antibacterial capability of the UgiGel against two pathogenic bacterial strains: P. aeruginosa (Gram-negative) and MRSA (Gram-positive) (Figure 3G). We used gelatin and bacteria without treatment as control groups. Throughout a 7-day incubation period, the OD measurements were used to assess bacterial growth and viability. As shown in Figure 3H,I, the control groups, consisting of untreated bacteria and gelatin, displayed a continuous increase in bacterial density throughout the experiment for both strains. In contrast, the bacteria cultured with UgiGel exhibited significantly reduced viability, as evidenced by much lower OD values. For S. aureus, the OD of UgiGel-treated samples showed a marked reduction compared to both the control and gelatin-treated samples, indicating strong antibacterial effects. Similarly, UgiGel demonstrated even more pronounced antibacterial activity against P. aeruginosa, where bacterial growth was almost completely inhibited by day 2 (OD  $\approx$  0.05). Also, the antibacterial activity at day 7  $(OD \approx 0.1)$  was far below the untreated bacteria  $(OD \approx 0.9)$  and gelatin (OD  $\approx$  0.8) groups.

#### 3.6 | In Vitro Antioxidant Activity of the UgiGel

The antioxidant activity of UgiGel was assessed through free radical scavenging assays [38]. UgiGel exhibited antioxidative activity, which was observed through a reduction in DPPH signal upon incubation with UgiGel likely due to hydrogen atom transfer or electron donation from UgiGel to DPPH radicals. The hydrogel demonstrated a free radical (DPPH)-scavenging efficiency of  $39.1 \pm 0.2$  after  $30\,\text{min}$  of incubation, confirming the antioxidant efficacy of UgiGel (Figure S3).

# 3.7 | In Vitro Biocompatibility and Degradation Study

We examined the in vitro biocompatibility of UgiGel by 2D seeding NIH-3T3 fibroblast cells on the surface of the hydrogel [44]. On days 1, 3, and 7 post-seeding, live/dead staining was conducted on cells seeded on either GelMA (control) or UgiGel. Both hydrogels supported cell viability (Figure 4A) [45], with more than 90% cell viability throughout the culture period (Figure 4B). At the same post-seeding timepoints, F-actin/DAPI staining was conducted to monitor cell morphology and proliferation. Both GelMA and UgiGel had increasing amounts of cells from day 1 to day 7 with healthy morphology (fibroblastic with well-organized F-actin filaments surrounding the nuclei) (Figure 4C) [46]. From the representative F-actin/DAPI images, cell number was determined to be progressively increasing for cells seeded on GelMA or UgiGel throughout the 7-day culture (Figure 4D). In particular, the cell numbers on UgiGel increased from 874.4 ± 124.2 number/ mm<sup>2</sup> on day 5 to  $1958 \pm 188.2$  number/mm<sup>2</sup> on day 7 comparable to GelMA.

## 3.8 | In Vivo Biocompatibility and Biodegradation of the UgiGel

To assess the in vivo biocompatibility and biodegradation of UgiGel, we conducted subcutaneous implantation of the lyophilized hydrogels in the dorsal tissue of rats (Figure 5A). After 7 and 28 days of implantation, the hydrogels were explanted with surrounding tissue for biodegradation monitoring and also for immunohistochemical analysis. H&E staining from the tissue/hydrogel interfaces revealed no signs of fibrosis or necrosis for both UgiGel and GelMA over the course of the 28-day implantation (Figure 5B). Furthermore, UgiGel robustly adhered to the tissue after 28 days, and cells appeared to migrate into the hydrogel matrix as it degraded. Black arrows indicated the nuclei that infiltrated into the UgiGel scaffold, suggesting the potential of UgiGel as a tissue-regenerating matrix. There was considerably more cell infiltration in the UgiGel scaffold compared to the control. For example, on day 28, the cell infiltration in UgiGel was at a density of  $9.5 \pm 0.6 \text{ cells/cm}^2$  whereas for GelMA it was  $4.8 \pm 0.7 \text{ cells/}$ cm<sup>2</sup> (Figure S4A). Also, cell infiltration increased within the UgiGel hydrogel during this time from  $2.9 \pm 0.2$  cells/cm<sup>2</sup> on day 7 to  $9.5 \pm 0.6$  cells/cm<sup>2</sup> on day 28.

Immunostaining for macrophages (through CD68 biomarkers) was performed to assess the local immune response to the implants (Figure 5C). We observed that there was an insignificant difference between the amount of macrophage infiltration on day 7  $(4.5\pm0.1 \text{ cells/cm}^2)$  compared to day 28  $(3.4\pm0.3 \text{ cells/}$ cm<sup>2</sup>) post-implantation in the tissue surrounding UgiGel (Figure S4B). UgiGel had a comparable immune response compared to GelMA, without any increase in macrophage activation during the 28-day implantation. In addition, we did not notice any negative effect of UgiGel on the general health and behavior of the rats, and all wounds on the implant site seemed to close normally. Additionally, UgiGel underwent in vivo biodegradation over the course of the subcutaneous implantation, where it degraded  $32.9\% \pm 8.6\%$  by day 7 and  $51.1\% \pm 12.4\%$  by day 28 (Figure 5D). The inset images provide a visual representation of UgiGel explanted on days 7 and 28, illustrating the progressive breakdown of the material over time. As the subcutaneously implanted hydrogels degraded, we measured the amount of macrophage infiltration by counting the CD68-stained cells (dyed red) based on immunostaining images.

#### 4 | Discussion

The Ugi-4CR has been widely explored for its versatility in functionalizing diverse materials such as carbon nanotubes (CNTs) [23, 47], graphene oxide [31], phthalocyanines [25], and natural polymers [26]. Recently, we demonstrated that the introduction of polyphenolic groups to a photocurable gelatin-based hydrogel significantly enhanced its elasticity and tissue adhesion properties [48]. However, the use of UV light and toxic photoinitiators in the formulation of these bioadhesives raises concerns about their clinical applicability, as such components may limit their safety and efficacy in medical settings [41]. Typically, multifunctional hydrogels are developed from a variety of polymers that are synthesized through complex, multistep processes. Although these multistep functionalization approaches have

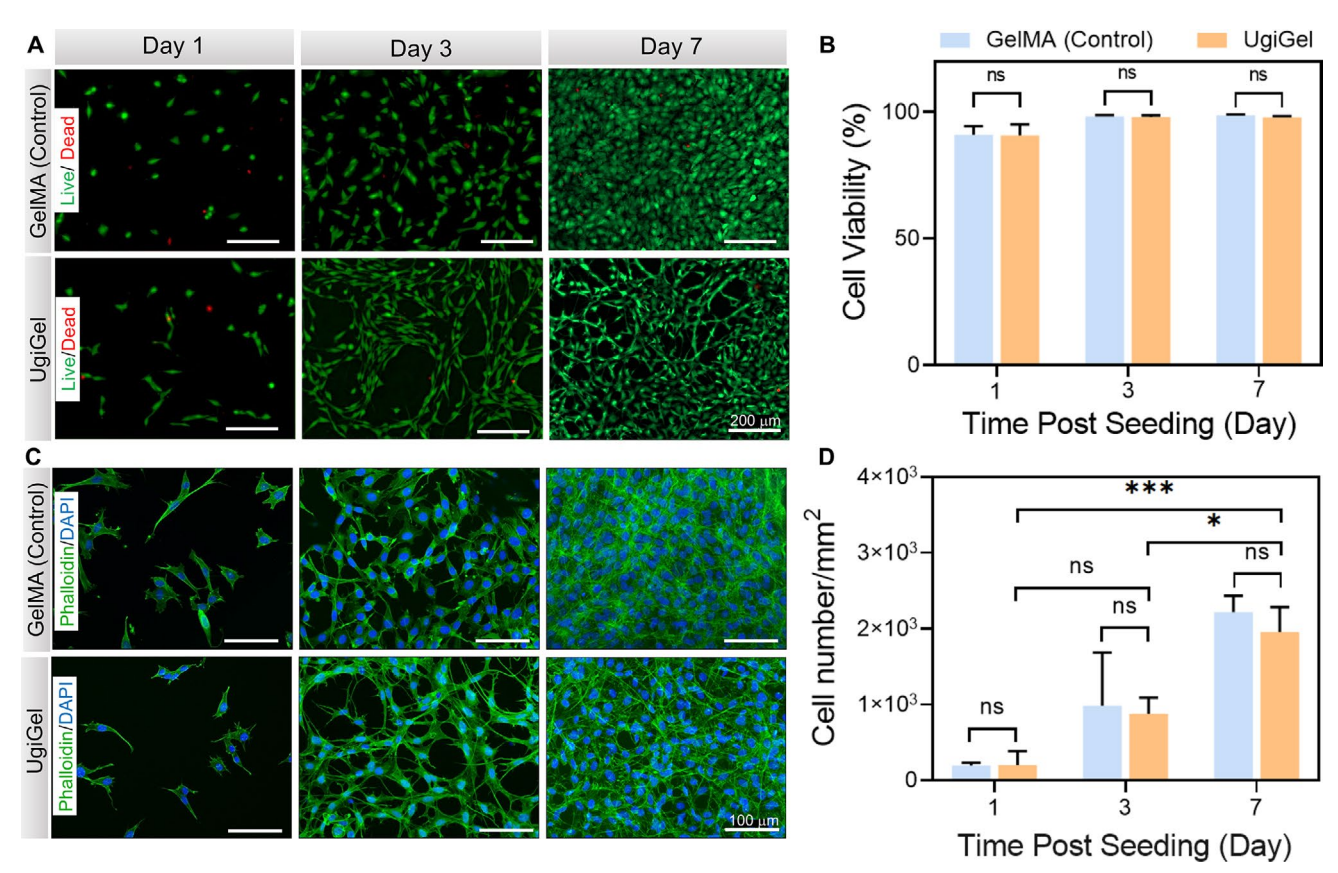


**FIGURE 4** | In vitro biocompatibility of UgiGel. (A) Representative live/dead stained images of NIH/3T3 cells seeded on UgiGel and a 10% (w/v) GelMA bioadhesive (control), taken on days 1, 3, and 7 post-seeding (scale bar:  $200\,\mu\text{m}$ ). (B) Quantitative analysis of NIH/3T3 cell viability at days 1, 3, and 7 post-seeding, showing no significant difference between UgiGel and GelMA at all time points. (C) Representative F-Actin/DAPI-stained images of NIH/3T3 cells seeded on UgiGel and GelMA, showing cell spreading and attachment at days 1, 3, and 7 post-seeding (scale bar:  $100\,\mu\text{m}$ ). (D) Quantitative cell density measurements (cells/mm²) at days 1, 3, and 7 post-seeding showing a significant increase in cell number on both UgiGel and GelMA over 7 days of culture (n=3, \*p<0.05, \*\*\*p<0.001).

been employed to prepare bioadhesive hydrogels, a one-pot, multicomponent approach has not been previously reported. In this study, for the first time, we addressed this challenge by developing a multifunctional gelatin-based bioadhesive functionalized via Ugi-4CR in a one-pot process under mild reaction conditions.

In our approach, gelatin served as the biocompatible backbone, while 4-FPBA, GA, and CyIso were incorporated to introduce various functional properties. Gelatin, well-known for its biocompatibility, is an ideal material for wound-healing applications [49]. GA, a phenolic compound found in plants, fruits, and leaves, offers numerous therapeutic benefits, including antioxidant, anti-inflammatory, analgesic, anticancer, and antidiabetic effects [50, 51]. The effectiveness of GA in promoting wound healing, particularly by enhancing cell migration in hyperglycemic conditions, has also been well documented [52]. Additionally, 4-FPBA exhibits wound-healing properties and demonstrates antibacterial activity against bacterial pathogens commonly associated with diabetic foot ulcers [53]. By integrating these components, our approach induces pseudopeptide structures, offering a multifunctional hydrogel with enhanced adhesive, antibacterial, antioxidant, and wound-healing capabilities.

A key feature of this study is the internal covalent crosslinking within the hydrogel network, which was facilitated by the dynamic boronate ester bonds formed between the 1,2- and 1,3-cis-diol groups of GA and the boronic groups of 4-FPBA, resulting in a mechanically stable UgiGel. Boronate ester formation is typically favored near or above the pKa of a given boronic acid, and in this case, the crosslinking occurred between the cis-diol groups of GA and the boronic acid groups on the gelatin backbone at physiological pH levels (≥7.4). This pH-dependent crosslinking allowed the formation of a stable UgiGel network without the need for light or chemical crosslinkers. To confirm that the internal crosslinking was specifically due to the presence of boronic groups, another reaction using the same aldehyde without boronic groups was also conducted. The absence of gel formation in this control experiment verified that the crosslinking and subsequent gelation were indeed attributed to the boronic groups of 4-FPBA. While previous studies have employed Ugi-4CR to synthesize boronic acid-containing gelators that form hydrogels by reacting with diol-containing polymers like PVA [28], these approaches often involve multiple steps and the use of different polymeric backbones. For example, Tao and coworkers synthesized PEG functionalized via Ugi-4CR and combined it with PVA to create an antibacterial, self-healing gel under mild conditions [29]. However, this method required three

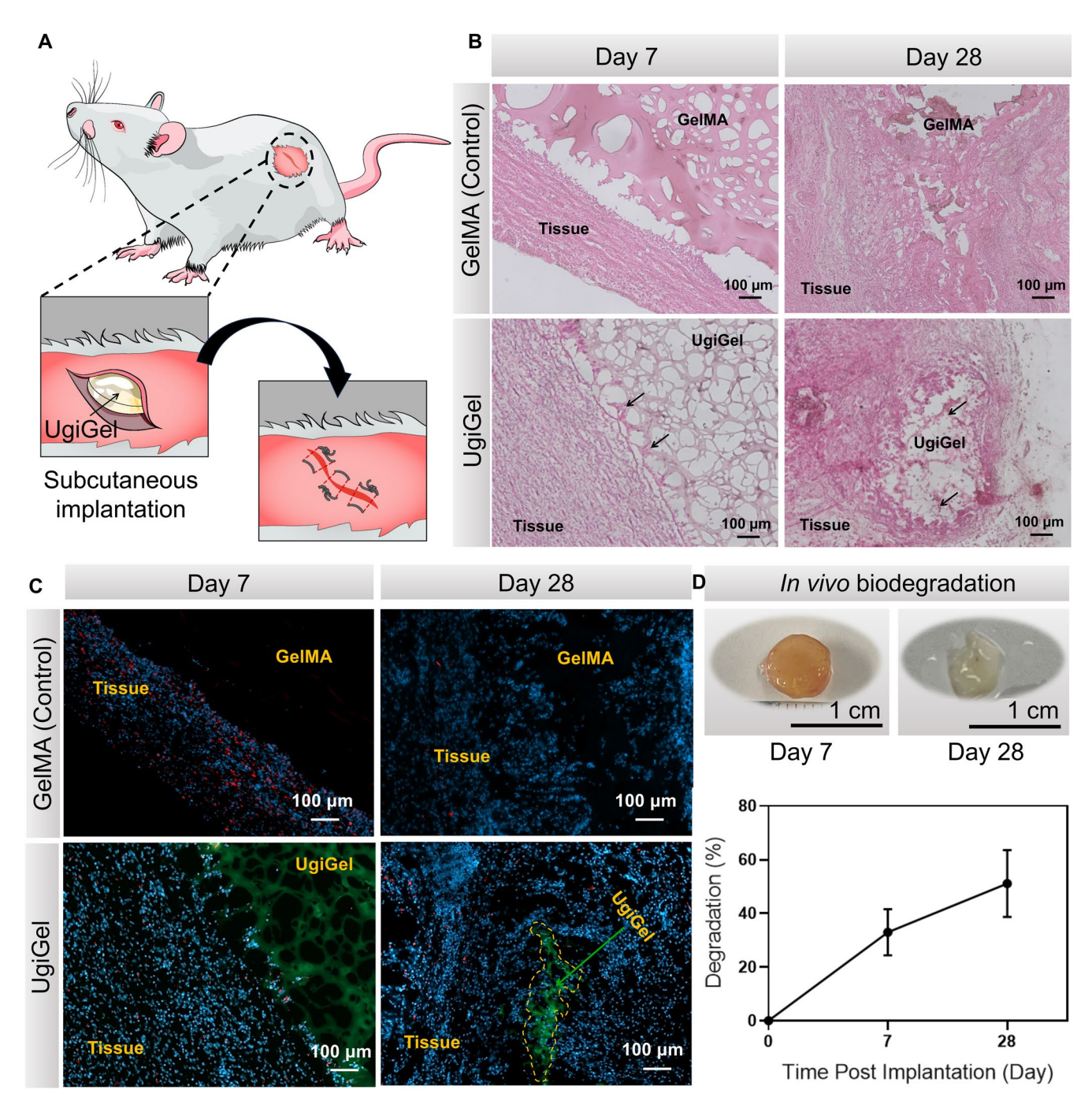


**FIGURE 5** | In vivo biocompatibility and biodegradation of UgiGel. (A) Schematic demonstration of subcutaneous implantation of UgiGel in rats. (B) Representative H&E-stained images of UgiGel/tissue interfaces at days 7 and 28 post-implantation, compared to 20% (w/v) GelMA bioadhesive as a control (black arrows indicate the nuclei infiltrated into the hydrogel scaffold). (C) Representative CD68/DAPI-stained images of the UgiGel/tissue interfaces at days 7 and 28 post-implantation. (D) Biodegradation profile of UgiGel over 28 days post-implantation. (n = 3, scale bar:100 µm).

distinct synthetic steps and the use of two separate polymers. In contrast, our design simplified the process by eliminating the need for external polymeric components and crosslinkers.

The ability of wound dressings to self-repair is critical in maintaining mechanical stability, preventing infection, and ensuring prolonged functionality. An ideal wound dressing must not only provide mechanical support but also minimize mechanical mismatch between the tissue and biomaterial, reducing immune responses and fibrotic tissue formation to facilitate functional tissue recovery [1]. Hydrogels without self-healing

properties may suffer some deformation or damage caused by external mechanical force after being applied to the wound site, undermining the integrity of the dressing as a protective barrier and causing bacteria to reach the wound area [54]. While several self-healing antibacterial hydrogels have been developed, many require complex photocrosslinking or multistep synthesis, limiting their clinical and commercial translation [55]. For instance, Chen et al. designed a self-healing hydrogel based on boronic-acid ester bonding, achieving nearly 100% fracture stress recovery within 48 h at room temperature. However, this system exhibited minimal stress relaxation and insignificant

residual deformation under repeated elongation cycles [56]. Commercial fibrin-based sealants such as Evicel and TISSEEL, as well as PEG-based Coseal, have established clinical safety but lack self-healing properties [57]. Despite advancements, to the best of our knowledge, no current self-healing hydrogel fully meets the demands of biocompatibility, antibacterial activity, mechanical robustness, and adaptability to the complex biological environment of wound healing. Moreover, the high cost of manufacturing self-healing hydrogels remains a significant barrier to widespread adoption. While natural polymerbased self-healing hydrogels offer cost advantages, scalable production remains a challenge [55]. Here, we leveraged the advantages of dynamic reversible boronate ester bonds to break and reform under appropriate conditions, enabling the UgiGel to recover after damage [58]. Additionally, the single-step synthesis process provided a cost-effective advantage. UgiGel also showed stretchability and flexibility, ensuring that the hydrogel can repair minor tears and maintain structural integrity, making it ideal for applications in wound healing, where flexibility and durability are crucial.

On the other hand, a slower degradation rate of bioadhesive at a physiological pH of 7.4, which is representative of the neutral environment typically found in skin and healing wounds, is crucial for effective wound healing [59]. This allows the hydrogel to maintain its mechanical strength and protective qualities throughout the healing process, preventing premature degradation. Since the early stages of wound healing typically last 3-4weeks, wound dressings must exhibit degradation profiles aligned with this timeframe [36]. In this study, UgiGel showed a degradation rate fitted within the required period for wound healing, maintaining structural integrity over time. Notably, UgiGel, fabricated without the use of light, catalysts, or chemical initiators, showed a gradual degradation of up to 42 days (76.6%  $\pm$  1.2%), making it suitable for wound sealing and repair. In addition to degradation, the swelling behavior of UgiGel a—key indicator of the stability of the hydrogel for biomedical applications [12], was assessed and exhibited an increase in swelling during the first  $10 \text{ h} (45.3\% \pm 2.6\%)$ , which remained stable until 48 h ( $46.7\% \pm 1.7\%$ ). The initial swelling phase can be attributed to physical and chemical factors. The gelatin backbone of UgiGel was naturally hydrophilic, and upon exposure to an aqueous environment, it absorbed water, leading to early swelling. In addition, the functionalization with GA and 4-FPBA through the Ugi-4CR introduced a network of amide bonds, further enhancing the hydrophilicity. The equilibrium between water absorption and the dynamic internal crosslinking stabilized the hydrogel structure, explaining the constant ratio after the initial phase.

Moreover, strong adhesion to wet tissue is a crucial factor in the design of bioadhesives to maintain tissue approximation, prevent dislocation, and ensure effective transmission of forces across the tissue–implant interface [60]. Inspired by the remarkable adhesion properties of mussels on wet surfaces, the role of polyphenol-modified pseudopeptide scaffolds in enhancing adhesive performance has been widely recognized [61]. Both GA and 4-FPBA contribute to the formation of strong adhesive networks, enabling marine organisms to securely attach to diverse surfaces, even in aqueous environments [62, 63]. Interestingly, as-prepared UgiGel showed strong adhesion to different surfaces like plastic, steel, and glass, which confirmed its adhesive

nature. Also, the wound closure test revealed that the adhesion strength of the UgiGel was significantly higher than that of GelMA bioadhesive and commercial sealants, Evicel and Coseal, due to the presence of a large amount of phenolic, hydroxyl, amine, and amide functional groups that can react with tissue functional groups such as carboxyl, hydroxyl, and amine groups, synergistically enhancing the adhesion of the gel network to the tissue surfaces. Notably, UgiGel adhesive strength was comparable to a previously published study that used a 10% GelMA hydrogel with varying concentrations of laponite [64]. In this study, the adhesive strength of the nanocomposite hydrogels increased from  $30.0 \pm 10.0$  to  $100.7 \pm 6.2$  kPa as the laponite concentration increased from 0% to 1%. However, the maximum adhesive strength reported,  $100.7 \pm 6.2 \,\mathrm{kPa}$ , was still lower than that of UgiGel, which was formed without any additional NPs. Our engineered polyphenol-functionalized UgiGel demonstrated superior adhesive properties within the optimal range of 50-200 kPa appropriate for skin wound closure [65]. This range provides sufficient adhesion to keep the dressing securely in place while still allowing for painless removal without causing additional damage to the wound tissue.

The sealing ability of UgiGel for the wound under liquid pressure was also evaluated ( $14.3\pm1.1\,\mathrm{kPa}$ ) and compared to commercial sealants (Coseal [ $1.7\pm0.1\,\mathrm{kPa}$ ] and Evicel [ $3.2\pm1.3\,\mathrm{kPa}$ ]) which showed higher burst pressure. In our previous study on the functionalization of gelatin with polydopamine [35], we reported a bioadhesive containing a high content of polyphenolic groups with a burst pressure of approximately  $15-20\,\mathrm{kPa}$ , depending on the concentration of the chemical crosslinker (NaIO<sub>4</sub>). In contrast, UgiGel achieved a comparable burst pressure without requiring any chemical crosslinker. This enhanced burst pressure highlights the potential of UgiGel as an effective bioadhesive for sealing dynamic tissues such as lungs and blood vessels.

When skin is impaired, bacteria can quickly infiltrate into underlying tissues, leading to life-threatening infections [66]. Previous studies have shown that polyphenol motifs present in the GA structure exhibit strong antibacterial activities. The phenolic groups can bind to proteins on bacterial membranes to change the permeability of bacterial membranes, thereby inhibiting the absorption of glucose and/or changing the ion concentrations inside and outside the membranes [48]. Additionally, PBA derivatives can bind to proteins on the bacterial membranes to inhibit their growth [67]. Leveraging these characteristics, we examined the antibacterial efficacy of the UgiGel, which showed efficacy against both Gram-positive and Gram-negative bacteria.

Typically, to impart antibacterial activity to bioadhesives, various metal NPs such as copper (Cu) or silver (Ag) have been incorporated into the hydrogel networks. For example, the addition of Cu<sup>2+</sup> to GelMA composites containing acrylated adenine demonstrated antibacterial activity, whereas composites without metal lacked antibacterial properties [68]. The antibacterial efficacy of the engineered hydrogels was dependent on the Cu<sup>2+</sup> concentration, with higher Cu<sup>2+</sup> levels leading to a lower bacterial survival rate. He et al. developed an antibacterial hydrogel incorporating Ag NPs, which, upon co-incubation with *E. coli*, led to approximately a 1.25-fold reduction in CFUs [69]. An antibacterial hydrogel incorporating Ag NPs and zinc oxide was fabricated, which, based

on OD measurements, reduced E. coli viability by 80%-95% and S. aureus viability by 40%–100% [70]. It is also proven that various metal-organic frameworks (MOFs) embedded in PEG-based hydrogels could prevent the proliferation of E. coli and S. aureus after 24h of treatment [71]. While the gels almost completely prevented the growth of E. coli, they caused around 80%-100% reduction of S. aureus OD. Even though the hydrogels exhibited antibacterial properties, their in vitro biocompatibility ranged from 20% to 70% cellular viability. In addition, in our previous study on gelatin functionalized with polydopamine, greater antibacterial efficacy was observed against the Gram-positive bacterium S. aureus compared to E. coli [35]. However, the engineered UgiGel exhibited higher antibacterial activity against Gram-negative bacteria compared to Gram-positive strains. In both cultures, we observed that treatment with UgiGel resulted in significantly lower OD compared to the untreated control on days 2 and 7 after the start of the co-incubation (\*p<0.0001). After the 7-day antibacterial test, the concentration of *P. aeruginosa* in the UgiGel-treated samples was about nine-fold less than the control, indicating a cessation of bacterial viability. Similarly, the concentration of S. aureus in the UgiGel-treated samples was more than two-fold less than that of the control. Therefore, we concluded the ability of UgiGel to prevent bacterial proliferation. This enhanced antibacterial effect could be attributed to the presence of phenolic groups from both 4-FPBA and GA, which bind to proteins on bacterial membranes. This interaction alters the ion concentrations within the membrane, disrupting essential processes and ultimately inhibiting bacterial growth. The dual-functionalization of gelatin with these polyphenol groups thus confers UgiGel with superior antimicrobial efficiency, making it a promising material for wound-healing applications where infection prevention is critical.

In addition, the development of wound dressings with antioxidant properties is essential for enhancing wound healing by neutralizing excess free radicals, thereby reducing oxidative stress at the wound site [72]. Excessive levels of reactive oxygen species (ROS) can hinder the healing process and cause cellular damage. By integrating antioxidants into wound dressings, ROS-induced damage is mitigated, creating a more favorable environment for tissue regeneration and reducing inflammation [73]. This strategy not only accelerates healing but also minimizes scar formation, making antioxidant-enriched dressings particularly advantageous for chronic and diabetic wounds. GA, a potent phenolic compound, with strong radical scavenging activity attributed to its ability to donate hydrogen atoms or electrons to neutralize free radicals, provides antioxidant properties [74]. Similarly, 4-FPBA has been shown to possess antioxidant properties [75]. Given the presence of both GA and 4-FPBA in UgiGel, we examined the antioxidant activity of UgiGel, which showed moderate antioxidative activity (39.1  $\pm$  0.2 after 30 min of incubation). The reason for this moderate activity might be due to the fact that most of the potential phenolic groups were involved in covalent and noncovalent bonding, which may cause a decrease in the antioxidant activity. These results suggest the efficacy of the Ugi-4CR in integrating functional components that contribute to the antioxidative properties of the hydrogel, further enhancing its potential as a therapeutic wound dressing.

The in vitro cytocompatibility of biomaterials is critical for their biomedical applications, including their use as bioadhesives. In

this study, UgiGel demonstrated excellent biocompatibility using NIH-3T3 fibroblast cells, supporting more than 90% cell viability for up to 7 days, which is comparable to the well-established GelMA bioadhesive. F-actin/DAPI staining revealed an increasing number of cells on UgiGel from day 1 to day 7, with cells displaying healthy fibroblastic morphology and well-organized F-actin filaments surrounding the nuclei. The cell density on UgiGel increased significantly, from 874.4 ± 124.2 cells/mm<sup>2</sup> on day 5 to  $1958 \pm 188.2$  cells/mm<sup>2</sup> on day 7, comparable to the results observed with GelMA. These observations confirmed that UgiGel can provide a supportive environment for cellular attachment, proliferation, and maintenance of cytoskeletal architecture. This could be attributed to the multifunctional components introduced via the MCR approach, which allowed for the creation of bioinspired pseudopeptide scaffolds. Importantly, the fabrication of UgiGel was free of light, catalysts, or chemical initiators, further enhancing its appeal as a biocompatible, environmentally benign material suitable for biomedical applications.

Currently, the only gelatin-based wound healer on the market is gelatin-resorcin-formalin (GRF) glue, which is significantly limited due to concerns about cytotoxicity caused by the release of formaldehyde during degradation [76]. Despite some successful outcomes, the use of glutaraldehyde in these formulations poses safety risks, as it is classified as a toxic substance, preventing FDA approval of GRF/GRFG glues in the United States. Furthermore, GRF lacks intrinsic antibacterial and antioxidant properties. In contrast, our novel design utilized the Ugi 4-CR to safely incorporate potentially toxic components, such as aldehyde and isocyanide derivatives, into a bioadhesive. This is achieved by forming stable amide bonds through the Mumm rearrangement. As a result, the toxicity of these individual components was neutralized, and the final product is a multifunctional, biocompatible adhesive with no detectable cytotoxic effects [18].

In vivo biocompatibility studies are critical for understanding possible adverse host immune responses that can occur due to the presence of the biomaterial or degradation byproducts. Furthermore, monitoring in vivo biodegradation in the presence of enzymes and immune cells can provide an assessment of the feasibility of using the engineered biomaterial for tissue engineering. Proper tissue integration without excessive scarring is vital for wound healing since gradual degradation can support the healing process by providing structural integrity [77]. In our study, H&E staining of the tissue/hydrogel interface showed no signs of fibrosis or necrosis for UgiGel over the 28-day implantation period. UgiGel remained robustly adhered to the tissue throughout this period, with evidence of cell migration into the hydrogel matrix as it gradually degraded. Notably, UgiGel demonstrated integration with the surrounding tissue better than the GelMA bioadhesive, which exhibited less cell infiltration. The immune response of UgiGel was also comparable to GelMA which is known or its high biocompatibility. Previously engineered hydrogels based on GelMA exhibited 30% degradation over 28 days unless the hydrogel was embedded with vascular-derived extracellular matrix (ECM), in which case it degraded 75% over the same timeframe of subcutaneous implantation [78]. We also studied the in vivo degradation profile of GelMA bioadhesive, which degraded 20% over 28 days, as well as of catechol-modified GelMA, which degraded 80% over the

same duration [79]. These findings demonstrate that UgiGel is both biocompatible and biodegradable, with a degradation profile that aligns well with the tissue healing timeline.

#### 5 | Conclusion

In conclusion, we successfully developed a multifunctional bioadhesive, UgiGel, through a one-pot Ugi-4CR synthesis, eliminating the need for light activation or crosslinkers. UgiGel demonstrated exceptional self-healing capabilities, high stretchability, and strong adhesion to various surfaces, including steel, gloves, and biological tissues. Notably, it achieved superior tissue adhesion strength (139.8 ± 8.7 kPa) on porcine skin compared to GelMA bioadhesive and commercial alternatives such as Evicel  $(20.8 \pm 76.7 \,\mathrm{kPa})$  and Coseal  $(26.3 \pm 4.7 \,\mathrm{kPa})$ . Its strong burst pressure performance further highlights its potential to effectively seal internal organs, such as blood vessels and lungs. UgiGel also exhibited robust antibacterial activity, showing significant efficacy against P. aeruginosa and S. aureus. Both in vitro and in vivo studies confirmed its biocompatibility, biodegradability, and favorable integration with surrounding tissue, making it a promising candidate for biomedical applications. UgiGel holds great potential for wound sealing and repair, and tissue engineering, offering a versatile and safe solution for various healthcare needs.

#### **Author Contributions**

Conceptualization: Ronak Afshari and Nasim Annabi. Formal analysis: Ronak Afshari, Arpita Roy, Saumya Jain, Kaimana Lum, Joyce Huang, and Sam Denton. Funding acquisition: Nasim Annabi. Investigation: Ronak Afshari, Arpita Roy, Saumya Jain, and Joyce Huang. Methodology: Ronak Afshari, Arpita Roy, Saumya Jain, Kaimana Lum, Joyce Huang, and Sam Denton. Project administration: Ronak Afshari and Nasim Annabi. Supervision: Ronak Afshari and Nasim Annabi. Validation: Ronak Afshari, Arpita Roy, Saumya Jain, Joyce Huang, and Nasim Annabi. Visualization: Arpita Roy and Ronak Afshari. Writing – original draft: Ronak Afshari. Writing – review and editing: Ronak Afshari, Arpita Roy, Saumya Jain, Joyce Huang, and Nasim Annabi. The manuscript was approved by all authors.

#### Acknowledgments

We acknowledge Yuting Zheng for helping with in vivo experiments. We acknowledge the support from the National Institutes of Health (R01-EB023052; R01-HL140618).

#### **Conflicts of Interest**

Dr. Nasim Annabi holds equity in GelMEDIX Inc. The remaining authors declare no conflicts of interest.

## Data Availability Statement

The data presented in this study are available on request from the corresponding author.

#### References

1. K. Las Heras, M. Igartua, E. Santos-Vizcaino, and R. M. Hernandez, "Chronic Wounds: Current Status, Available Strategies and Emerging Therapeutic Solutions," *Journal of Controlled Release* 328 (2020): 532–550.

- 2. L. J. Borda, F. E. Macquhae, and R. S. Kirsner, "Wound Dressings: A Comprehensive Review," *Current Dermatology Reports* 5, no. 4 (2016): 287–297.
- 3. V. Brumberg, T. Astrelina, T. Malivanova, et al., "Modern Wound Dressings: Hydrogel Dressings," *Biomedicines* 9, no. 9 (2021): 1235.
- 4. S. Rathi, R. Saka, A. J. Domb, and W. Khan, "Protein-Based Bioadhesives and Bioglues," *Polymers for Advanced Technologies* 30, no. 2 (2019): 217–234.
- 5. G. M. Taboada, K. Yang, M. J. N. Pereira, et al., "Overcoming the Translational Barriers of Tissue Adhesives," *Nature Reviews Materials* 5, no. 4 (2020): 310–329.
- 6. R. Pinnaratip, M. S. A. Bhuiyan, K. Meyers, R. M. Rajachar, and B. P. Lee, "Multifunctional Biomedical Adhesives," *Advanced Healthcare Materials* 8, no. 11 (2019): 1801568.
- 7. A. A. P. Mansur, M. A. Rodrigues, N. S. V. Capanema, S. M. Carvalho, D. A. Gomes, and H. S. Mansur, "Functionalized Bioadhesion-Enhanced Carboxymethyl Cellulose/Polyvinyl Alcohol Hybrid Hydrogels for Chronic Wound Dressing Applications," *RSC Advances* 13, no. 19 (2023): 13156–13168.
- 8. L. Zhang, M. Liu, Y. Zhang, and R. Pei, "Recent Progress of Highly Adhesive Hydrogels as Wound Dressings," *Biomacromolecules* 21, no. 10 (2020): 3966–3983.
- 9. L. Zhao, Z. Shi, X. Sun, et al., "Natural Dual-Crosslinking Bioadhesive Hydrogel for Corneal Regeneration in Large-Size Defects," *Advanced Healthcare Materials* 11, no. 21 (2022): 2201576.
- 10. R. Song, X. Wang, M. Johnson, et al., "Enhanced Strength for Double Network Hydrogel Adhesive Through Cohesion-Adhesion Balance," *Advanced Functional Materials* 34, no. 23 (2024): 2313322.
- 11. Y. Liu, Y. Ouyang, L. Yu, et al., "Novel Approach for Enhancing Skin Allograft Survival by Bioadhesive Nanoparticles Loaded With Rapamycin," *International Journal of Pharmaceutics* 651 (2024): 123742.
- 12. Y. Zheng, K. Shariati, M. Ghovvati, et al., "Hemostatic Patch With Ultra-Strengthened Mechanical Properties for Efficient Adhesion to Wet Surfaces," *Biomaterials* 301 (2023): 122240.
- 13. S. Bashir, M. Hina, J. Iqbal, et al., "Fundamental Concepts of Hydrogels: Synthesis, Properties, and Their Applications," *Polymers* 12, no. 11 (2020): 2702.
- 14. M. Santos, T. Cernadas, P. Martins, et al., "Polyester-Based Photocrosslinkable Bioadhesives for Wound Closure and Tissue Regeneration Support," *Reactive and Functional Polymers* 158 (2021): 104798.
- 15. R. Afshari and A. Shaabani, "Materials Functionalization With Multicomponent Reactions: State of the Art," ACS Combinatorial Science 20, no. 9 (2018): 499–528.
- 16. T. Zarganes-Tzitzikas, A. L. Chandgude, and A. Dömling, "Multi-component Reactions, Union of MCRs and Beyond," *Chemical Record* 15, no. 5 (2015): 981–996.
- 17. A. Dömling, W. Wang, and K. Wang, "Chemistry and Biology of Multicomponent Reactions," *Chemical Review* 112, no. 6 (2012): 3083–3135.
- 18. A. Dömling, "Recent Developments in Isocyanide Based Multicomponent Reactions in Applied Chemistry," *Chemical Reviews* 106, no. 1 (2006): 17–89.
- 19. S. E. Hooshmand and W. Zhang, "Ugi Four-Component Reactions Using Alternative Reactants," *Molecules* 28, no. 4 (2023): 1642.
- 20. A. Sehlinger, P. K. Dannecker, O. Kreye, and M. A. R. Meier, "Diversely Substituted Polyamides: Macromolecular Design Using the Ugi Four-Component Reaction," *Macromolecules* 47, no. 9 (2014): 2774–2783.
- 21. I. Ugi, B. Werner, and A. Dömling, "The Chemistry of Isocyanides, Their Multi Component Reactions and Their Libraries," *Molecules* 8, no. 1 (2003): 53–66.

- 22. B. Yang, Y. Zhao, X. Ren, et al., "The Power of One-Pot: A Hexa-Component System Containing  $\pi$ – $\pi$  Stacking, Ugi Reaction and RAFT Polymerization for Simple Polymer Conjugation on Carbon Nanotubes," *Polymer Chemistry* 6, no. 4 (2014): 509–513.
- 23. A. Shaabani and R. Afshari, "Synthesis of Carboxamide-Functionalized Multiwall Carbon Nanotubes via Ugi Multicomponent Reaction: Water-Dispersible Peptidomimetic Nanohybrid as Controlled Drug Delivery Vehicle," *ChemistrySelect* 2, no. 18 (2017): 5218–5225.
- 24. A. Rezaei, O. Akhavan, E. Hashemi, and M. Shamsara, "Toward Chemical Perfection of Graphene-Based Gene Carrier via Ugi Multicomponent Assembly Process," *Biomacromolecules* 17, no. 9 (2016): 2963–2971
- 25. R. Afshari, V. Ghasemi, S. Shaabani, A. Shaabani, Z. Aladaghlo, and A. R. Fakhari, "Post-modification of Phthalocyanines via Isocyanide-Based Multicomponent Reactions: Highly Dispersible Peptidomimetic Metallophthalocyanines as Potent Photosensitizers," *Dyes and Pigments* 166 (2019): 49–59.
- 26. L. Reguera, Y. Méndez, A. R. Humpierre, O. Valdés, and D. G. Rivera, "Multicomponent Reactions in Ligation and Bioconjugation Chemistry," *Account of Chemical Research* 51, no. 6 (2018): 1475–1486.
- 27. H. Yazdani, S. E. Hooshmand, and M. H. Stenzel, "Fusion of Cellulose and Multicomponent Reactions: Benign by Design," *ACS Sustainable Chemistry & Engineering* 10, no. 14 (2022): 4359–4373.
- 28. Y. Zeng, C. Zhu, L. Tao, Y. Zeng, L. Tao, and C. Zhu, "Stimuli-Responsive Multifunctional Phenylboronic Acid Polymers Via Multicomponent Reactions: From Synthesis to Application," *Macromolecular Rapid Communications* 42, no. 18 (2021): 2100022.
- 29. Y. Zeng, Y. Li, G. Liu, Y. Wei, Y. Wu, and L. Tao, "Antibacterial Self-Healing Hydrogel via the Ugi Reaction," *ACS Applied Polymer Materials* 2, no. 2 (2020): 404–410.
- 30. W. Zhang, P. Tang, M. A. Abubaker, G.-H. Hu, and F.-E. Chen, "Advances of Ugi Reaction in Natural Product Synthesis," *Green Synthesis and Catalysis* (2024), https://doi.org/10.1016/j.gresc.2024.08.004.
- 31. A. Shaabani and R. Afshari, "Magnetic Ugi-Functionalized Graphene Oxide Complexed With Copper Nanoparticles: Efficient Catalyst toward Ullman Coupling Reaction in Deep Eutectic Solvents," *Journal of Colloid and Interface Science* 510 (2018): 384–394.
- 32. C. Jumelle, E. S. Sani, Y. Taketani, et al., "Growth Factor-Eluting Hydrogels for Management of Corneal Defects," *Materials Science and Engineering: C* 120 (2021): 111790.
- 33. C. Jumelle, A. Yung, E. S. Sani, et al., "Development and Characterization of a Hydrogel-Based Adhesive Patch for Sealing Open-Globe Injuries," *Acta Biomaterialia* 137 (2022): 53–63.
- 34. Y. Zhu, Q. Luo, H. Zhang, et al., "A Shear-Thinning Electrostatic Hydrogel With Antibacterial Activity by Nanoengineering of Polyelectrolytes," *Biomaterials Science* 8, no. 5 (2020): 1394–1404.
- 35. H. Montazerian, A. Hassani Najafabadi, E. Davoodi, et al., "Poly-Catecholic Functionalization of Biomolecules for Rapid Gelation, Robust Injectable Bioadhesion, and Near-Infrared Responsiveness," *Advanced Healthcare Materials* 12, no. 17 (2023): 2203404.
- 36. N. Annabi, D. Rana, E. Shirzaei Sani, et al., "Engineering a Sprayable and Elastic Hydrogel Adhesive With Antimicrobial Properties for Wound Healing," *Biomaterials* 139 (2017): 229–243.
- 37. A. Roy, P. Guha Ray, A. Bose, S. Dhara, and S. Pal, "PH-Responsive Copolymeric Network Gel Using Methacrylated β-Cyclodextrin for Controlled Codelivery of Hydrophilic and Hydrophobic Drugs," *ACS Applied Bio Materials* 5, no. 7 (2022): 3530–3543.
- 38. A. Roy, P. Guha Ray, K. Manna, C. Banerjee, S. Dhara, and S. Pal, "Poly(N-Vinyl Imidazole) Cross-Linked  $\beta$ -Cyclodextrin Hydrogel for Rapid Hemostasis in Severe Renal Arterial Hemorrhagic Model," *Biomacromolecules* 22, no. 12 (2021): 5256–5269.

- 39. N. Annabi, S. M. Mithieux, P. Zorlutuna, G. Camci-Unal, A. S. Weiss, and A. Khademhosseini, "Engineered Cell-Laden Human Protein-Based Elastomer," *Biomaterials* 34, no. 22 (2013): 5496–5505.
- 40. N. Annabi, K. Tsang, S. M. Mithieux, et al., "Highly Elastic Micropatterned Hydrogel for Engineering Functional Cardiac Tissue," *Advanced Functional Materials* 23, no. 39 (2013): 4950–4959.
- 41. N. Annabi, Y. N. Zhang, A. Assmann, et al., "Engineering a Highly Elastic Human Protein-Based Sealant for Surgical Applications," *Science Translational Medicine* 9, no. 410 (2017): aai7466.
- 42. M. Zhu, W. Li, X. Dong, et al., "In Vivo Engineered Extracellular Matrix Scaffolds With Instructive Niches for Oriented Tissue Regeneration," *Nature Communication* 10, no. 1 (2019): 4620.
- 43. Y. Mao, Y. Zhang, Y. Wang, T. Zhou, B. Ma, and P. Zhou, "A Multifunctional Nanocomposite Hydrogel With Controllable Release Behavior Enhances Bone Regeneration. *Regenerative*," *Biomaterials* 10 (2023): rbad046.
- 44. A. Roy, S. Zenker, S. Jain, et al., "A Highly Stretchable, Conductive, and Transparent Bioadhesive Hydrogel as a Flexible Sensor for Enhanced Real-Time Human Health Monitoring," *Advanced Materials* 36, no. 35 (2024): 2404225.
- 45. A. Assmann, A. Vegh, M. Ghasemi-Rad, et al., "A Highly Adhesive and Naturally Derived Sealant," *Biomaterials* 140 (2017): 115–127.
- 46. A. M. Rahimi, M. Cai, and S. Hoyer-Fender, "Heterogeneity of the NIH3T3 Fibroblast Cell Line," *Cells* 11, no. 17 (2022): 2677.
- 47. R. Afshari, S. Emad Hooshmand, M. Atharnezhad, and A. Shaabani, "An Insight into the Novel Covalent Functionalization of Multi-Wall Carbon Nanotubes With Pseudopeptide Backbones for Palladium Nanoparticles Immobilization: A Versatile Catalyst towards Diverse Cross-Coupling Reactions in Bio-Based Solvents," *Polyhedron* 175 (2020): 114238.
- 48. H. Montazerian, A. Baidya, R. Haghniaz, et al., "Stretchable and Bioadhesive Gelatin Methacryloyl-Based Hydrogels Enabled by In Situ Dopamine Polymerization," *ACS Applied Materials & Interfaces* 13, no. 34 (2021): 40290–40301.
- 49. J. I. Kang and K. M. Park, "Advances in Gelatin-Based Hydrogels for Wound Management," *Journal of Materials Chemistry B* 9, no. 6 (2021): 1503–1520.
- 50. A. Nouri, N. Salehi-Vanani, and E. Heidarian, "Antioxidant, Anti-Inflammatory and Protective Potential of Gallic Acid against Paraquat-Induced Liver Toxicity in Male Rats," *Avicenna Journal of Phytomedicine* 11, no. 6 (2021): 633.
- 51. N. A. Al Zahrani, R. M. El-Shishtawy, and A. M. Asiri, "Recent Developments of Gallic Acid Derivatives and Their Hybrids in Medicinal Chemistry: A Review," *European Journal of Medicinal Chemistry* 204 (2020): 112609.
- 52. D. J. Yang, S. H. Moh, D. H. Son, et al., "Gallic Acid Promotes Wound Healing in Normal and Hyperglucidic Conditions," *Molecules* 21, no. 7 (2016): 899.
- 53. H. M. U. Abid, M. Hanif, K. Mahmood, M. Aziz, G. Abbas, and H. Latif, "Wound-Healing and Antibacterial Activity of the Quercetin-4-Formyl Phenyl Boronic Acid Complex against Bacterial Pathogens of Diabetic Foot Ulcer," *ACS Omega* 7, no. 28 (2022): 24415–24422.
- 54. A. Zhang, Y. Liu, D. Qin, M. Sun, T. Wang, and X. Chen, "Research Status of Self-Healing Hydrogel for Wound Management: A Review," *International Journal of Biological Macromolecules* 164 (2020): 2108–2123.
- 55. P. Yang, Z. Li, B. Fang, and L. Liu, "Self-Healing Hydrogels Based on Biological Macromolecules in Wound Healing: A Review," *International Journal of Biological Macromolecules* 253 (2023): 127612.
- 56. Y. Chen, W. Qian, R. Chen, et al., "One-Pot Preparation of Autonomously Self-Healable Elastomeric Hydrogel From Boric Acid and

- Random Copolymer Bearing Hydroxyl Groups," ACS Macro Letters 6, no. 10 (2017): 1129–1133.
- 57. K. G. M. Brown and M. J. Solomon, "Topical Haemostatic Agents in Surgery," *British Journal of Surgery* 111, no. 1 (2024): znad361.
- 58. R. Dong and B. Guo, "Smart Wound Dressings for Wound Healing," *Nano Today* 41 (2021): 101290.
- 59. S. L. Percival, S. McCarty, J. A. Hunt, and E. J. Woods, "The Effects of PH on Wound Healing, Biofilms, and Antimicrobial Efficacy," *Wound Repair and Regeneration* 22, no. 2 (2014): 174–186.
- 60. A. Rudawska, ed., Adhesives Applications and Properties (InTech, 2016).
- 61. H. Cheng, K. Yue, M. Kazemzadeh-Narbat, et al., "Mussel-Inspired Multifunctional Hydrogel Coating for Prevention of Infections and Enhanced Osteogenesis," *ACS Applied Materials Interfaces* 9, no. 13 (2017): 11428–11439.
- 62. A. Basit, H. Yu, L. Wang, et al., "Recent Advances in Wet Surface Tissue Adhesive Hydrogels for Wound Treatment," *European Polymer Journal* 216 (2024): 113260.
- 63. Y. Lu, X. Xu, and J. Li, "Recent Advances in Adhesive Materials Used in the Biomedical Field: Adhesive Properties, Mechanism, and Applications," *Journal of Materials Chemistry B* 11, no. 15 (2023): 3338–3355.
- 64. N. Zandi, B. Dolatyar, R. Lotfi, et al., "Biomimetic Nanoengineered Scaffold for Enhanced Full-Thickness Cutaneous Wound Healing," *Acta Biomaterialia* 124 (2021): 191–204.
- 65. A. Gefen, P. Alves, D. Beeckman, et al., "How Should Clinical Wound Care and Management Translate to Effective Engineering Standard Testing Requirements From Foam Dressings? Mapping the Existing Gaps and Needs," *Advances in Wound Care (New Rochelle)* 13, no. 1 (2024): 34.
- 66. A. S. Moffarah, M. Mohajer Al, B. L. Hurwitz, and D. G. Armstrong, "Skin and Soft Tissue Infections," in *Diagnostic Microbiology of the Immunocompromised Host* (Wiley, 2016), 691–708.
- 67. S. Gao, Y. Zhang, R. Zhou, et al., "Boronic Acid-Assisted Detection of Bacterial Pathogens: Applications and Perspectives," *Coordination Chemistry Reviews* 518 (2024): 216082.
- 68. J. Chen, J. He, Y. Yang, et al., "Antibacterial Adhesive Self-Healing Hydrogels to Promote Diabetic Wound Healing," *Acta Biomaterialia* 146 (2022): 119–130.
- 69. X. He, Z. Li, J. Li, et al., "Ultrastretchable, Adhesive, and Antibacterial Hydrogel With Robust Spinnability for Manufacturing Strong Hydrogel Micro/Nanofibers," *Small* 17, no. 49 (2021): e2103521.
- 70. C. Mao, Y. Xiang, X. Liu, et al., "Photo-Inspired Antibacterial Activity and Wound Healing Acceleration by Hydrogel Embedded With Ag/Ag@AgCl/ZnO Nanostructures," *ACS Nano* 11, no. 9 (2017): 9010–9021.
- 71. K. Gwon, I. Han, S. Lee, Y. Kim, and D. N. Lee, "Novel Metal-Organic Framework-Based Photocrosslinked Hydrogel System for Efficient Antibacterial Applications," *ACS Applied Materials Interfaces* 12, no. 18 (2020): 20234–20242.
- 72. Z. Xu, S. Han, Z. Gu, and J. Wu, "Advances and Impact of Antioxidant Hydrogel in Chronic Wound Healing," *Advanced Healthcare Materials* 9, no. 5 (2020): 1901502.
- 73. G. Wang, F. Yang, W. Zhou, N. Xiao, M. Luo, and Z. Tang, "The Initiation of Oxidative Stress and Therapeutic Strategies in Wound Healing," *Biomedicine & Pharmacotherapy* 157 (2023): 114004.
- 74. P. S. Kaparekar, S. Pathmanapan, and S. K. Anandasadagopan, "Polymeric Scaffold of Gallic Acid Loaded Chitosan Nanoparticles Infused With Collagen-Fibrin for Wound Dressing Application," *International Journal of Biological Macromolecules* 165 (2020): 930–947.
- 75. Y. Liang, J. He, and B. Guo, "Functional Hydrogels as Wound Dressing to Enhance Wound Healing," *ACS Nano* 15, no. 8 (2021): 12687–12722.

- 76. S. Suzuki and Y. Ikada, "Sealing Effects of Cross-Linked Gelatin," *Journal of Biomaterials Applications* 27, no. 7 (2013): 801–810.
- 77. X. Cao, X. Wu, Y. Zhang, X. Qian, W. Sun, and Y. Zhao, "Emerging Biomedical Technologies for Scarless Wound Healing," *Bioactive Materials* 42 (2024): 449–477.
- 78. J. Chen, X. Zhou, W. Sun, et al., "Vascular Derived ECM Improves Therapeutic Index of BMP-2 and Drives Vascularized Bone Regeneration," *Small* 18, no. 36 (2022): 2107991.
- 79. S. Baghdasarian, B. Saleh, A. Baidya, et al., "Engineering a Naturally Derived Hemostatic Sealant for Sealing Internal Organs," *Materials Today Bio* 13 (2022): 100199.

#### **Supporting Information**

Additional supporting information can be found online in the Supporting Information section.